ADVANCED MATERIALS TECHNOLOGIES
www.advmattechnol.de

Highly Durable Membrane Electrode Assembly with Multiwalled Carbon Nanotubes/CeO_2-Reinforced Nafion Composite Membrane by Spraying Method for Fuel Cell Applications

*Eunho Choi, Sang Moon Kim, and Segeun Jang**

For achieving economically viable polymer electrolyte membrane fuel cells (PEMFCs) in the commercial market, simplifying the fabrication process and manufacturing of robust membrane electrode assembly (MEA) are important. Herein, a single spray-coating method for developing a robust and free-standing reinforced Nafion composite membrane and electrodes is reported. By comparing the fabricated membrane's morphology under diverse process conditions including the nozzle-to-substrate distance and solution-loading rates, the optimized spray-coating for uniformly deposited spray-based membrane without any defects has been determined. To explain this optimized condition, a simple theoretical model based on the concept of the surface coverage of sprayed droplets is proposed. The fabricated multiwalled carbon nanotubes/CeO_2-reinforced Nafion composite membrane shows excellent mechanical properties with minimal proton-conducting loss despite using additional fillers of total 4 wt% in the Nafion matrix. By successively depositing the catalyst layer on that membrane using the same spray-coating device, an MEA with the reinforced spray-based membrane has been successfully fabricated; moreover, diverse electrochemical measurements and durability tests have been conducted. The MEA with the reinforced membrane shows comparable initial performance and considerably higher performance after the durability test compared to the MEA with commercial Nafion membrane.

1. Introduction

Recently, hydrogen has received considerable attention as the most promising energy carrier enabling a clean and sustainable ecosystem by replacement of fossil fuels, which are accelerating global warming-induced environmental destruction. As ecofriendly energy conversion systems, polymer-electrolyte membrane fuel cells (PEMFCs) use the chemical energy of both hydrogen and oxygen to generate electricity with high efficiency, zero pollution, and rapid start-up/shut-down at relatively low temperatures (<100 °C).[1,2] Because of these attractive characteristics, PEMFCs have considerable potential as power sources for diverse applications, particularly in automobiles; With the motivation, many manufacturers have successfully commercialized these applications. However, some critical issues, such as high cost, insufficient durability, and water management difficulty, still limit further commercialization of PEMFCs in the market. Therefore, to address these issues, novel technological breakthroughs are necessary. Accordingly, the United States (US) Department of Energy (DOE) has set 2025 technical targets for membrane electrode assembly (MEA) in fuel cells. The targets require almost two times prolonged fuel cell durability to 8000 h and reduced MEA cost by 15% compared to those of the current commercial achievement of 4100 h and \$11.8 kW^{-1}.[3] MEA, which is the essential part of PEMFCs, where electrochemical reactions occur, comprises two catalyst layers (anode and cathode) and a proton exchange membrane (PEM).

Generally, MEA is manufactured by two representative techniques,[4] i.e., decal transfer and direct coating methods. For the decal transfer process, catalyst ink or slurry is first coated onto the release films. Next, at high pressure and temperature above the glass transition temperature of the PEM, the coated films are transferred to the PEM which is prepared by casting the electrolyte ionomer to the backer film. For the direct coating process, catalyst inks are directly coated onto the PEM by spray coating or ink-jet printing. For these processes, membrane manufacturing and electrode-coating should be separately conducted, and different type of equipment is required for each process. To simplify manufacturing, direct membrane deposition (DMD) method has been extensively studied.[5–10] For the DMD process, without the free-standing membrane, PEM is directly coated onto the anode and cathode in which the catalyst layer is coated on a gas diffusion layer (GDL) via a single coating system (e.g., spray or ink-jet), and then layers are assembled after aligning membrane-coated

E. Choi, S. Jang
School of Mechanical Engineering
Kookmin University
Seoul 02707, Republic of Korea
E-mail: sjang@kookmin.ac.kr
S. M. Kim
Department of Mechanical Engineering
Incheon National University
Incheon 22012, Republic of Korea
The ORCID identification number(s) for the author(s) of this article can be found under https://doi.org/10.1002/admt.202101360.

DOI: 10.1002/admt.202101360

surfaces to face each other. This DMD process has demonstrated high potential for reducing cost by eliminating the preparation steps of PEM films and using the single deposition process for fabricating MEA. Moreover, it has exhibited high performance using ultra-thin PEM with low ohmic resistance. However, it requires additional sub-gaskets with smaller openings than the catalyst-coated area for blocking the reactant gas crossover because of the non-use of a free-standing PEM which acts as a barrier for blocking the reactant gas crossover and electrical conduction.[6,8,10] Furthermore, the consecutive formation of the catalyst layer and the membrane in the DMD process was conducted on the GDL with an uneven surface of the microporous carbon layer, several protruded carbon fibers, and micrometer-sized cracks. This effect led to electric short-circuit characteristics, which can significantly affect the long-term operation of PEMFCs.[5,9]

Concerning the PEM, perfluorosulfonic acid (PFSA) membranes, such as Nafion, are extensively used for PEMFCs because of their high proton conductivity; however, during fuel cell operation, pure PFSA membranes suffer from high chemical and mechanical degradation.[11,12] In harsh operating conditions, such as repetitive wet/dry cycling environments (particularly automotive applications), PEM is exposed to severe mechanical stresses induced by repetitive swelling and shrinking.[13] Strategies for reinforcing the membrane via chemical polymer crosslinking, the impregnation of the electrolyte ionomer into porous polytetrafluoroethylene (PTFE) film[14,15] or electrospun polymer webs,[16] and insertion of inorganic/organic nanomaterials, such as TiO_2,[17] SiO_2,[18] hexagonal boron nitrides (h-BN),[19] GO layer,[5,20,21] graphene sheets,[22] and multiwalled carbon nanotubes (MWCNTs),[23–25] are extensively studied and proposed to improve mechanical stability. In particular, graphene and MWCNTs have been extensively used for mechanically reinforcing the membrane since their high mechanical properties provide the membrane with high stiffness (or elastic modulus) and dimensional stability. However, agglomeration issues induced by the rapid solvent evaporation and protrusion of materials with high electrical conductivity often cause electric crossover through the membrane when the membrane is fabricated by the conventional casting-drying method.[24–27] The chemical durability of PEM is primarily related to the formation of radicals, such as hydroxyl (HO•), and hydroperoxyl (HOO•), from Fenton's reaction of metal impurities in the system as well as hydrogen peroxides generated from incomplete oxygen reduction reaction (ORR) or crossover of reactants. These radicals cleave the sulfonic acid functional group and decompose the polymeric backbone of the PEM and ionomers in the catalyst layer, which shortens the lifetime of the PEMFC.[11,12] To mitigate the chemical degradation from radical attack, the strategy of incorporating radical scavengers, such as CeO_2, into the PEM has been extensively reported,[25,28,29] and this strategy is applied to commercially available membranes, such as Nafion XL, and presumably reinforced GORE membranes. The redox couple of Ce (III)/Ce (IV) can easily switch its oxidation state and can, therefore, quench the radicals.[14,29] However, technical issues still require to be addressed such as a significant decrease in the proton conductivity of the PEM and the ionomer because of the blockage of the proton transport by agglomerated CeO_2 nanoparticles and CeO_2 dissolution during operation.[14,30]

To deal with technical issues including developing a facile and simple MEA fabrication process and highly durable PEM, we propose a single spray-coating method for achieving a reinforced PEM with an even and uniform surface, which contains CeO_2 and MWCNTs, as well as successive manufacturing process for constructing a catalyst layer with the same equipment. The free-standing membrane can act as a mechanical support to the cell and a barrier for the crossover of reactants. There are not many previous studies for manufacturing spray-based free-standing membranes because of the difficulty in securing defects (e.g., pinhole)-free and uniform thickness membrane via droplet-based deposition, we established an optimal process for developing the membrane by varying the process condition. For acquiring a robust spray-based free-standing membrane, we carefully controlled the deposition conditions, including the spray travel path and moving speed, flow rate, gas pressure, nozzle-to-substrate distance, and spot size. Based on the observation of the membranes' surface morphologies and investigation, we could set the criteria for avoiding the formation of pinholes and agglomerated electrolyte particles by proposing a simple theoretical modeling, which confirms the experimental results. Furthermore, the additional incorporation of MWCNTs and CeO_2 provides mechanical and chemical durability to the PEM without agglomeration issues. Finally, the successive direct deposition of the catalyst to the prepared membrane was performed using the same single spray-coating device without using an expensive catalyst-coated release or membrane backer film in the conventional fabrication process. To demonstrate the excellence of the prepared PEM and MEA, their chemical, mechanical, and electrochemical characteristics were extensively measured and investigated.

2. Results and Discussion

2.1. MEA Fabrication with Single Spray-Coating

Figure 1a–d shows the schematic of experimental apparatus for developing the MWCNTs/CeO_2-reinforced Nafion composite membrane, and the successive MEA fabrication process via a lab-made single spray-coating device. The air brush was mounted to the commercial 3D printing machine by designing the jig to hold the spray handle and attach a screw to adjust the size of the nozzle's opening. First, to develop a defect-free and free-standing membrane with uniform thickness, process variables, including the flow rates, the carrier gas velocity, the nozzle-to-substrate distance, the spot-area size, the spray travel path, and the feeding rate, were carefully controlled. Then, a solution consisting of MWCNTs, CeO_2, Nafion ionomer, and a mixture of 1-propanol and deionized water was deposited onto the Si wafer substrate, which was fixed on a hotplate at temperature of 85 °C (Figure 1a). The fabricated MWCNTs/CeO_2-reinforced Nafion composite membrane were thermally treated by increasing and maintaining the hotplate temperature at 120 °C, which is the glass transition temperature of Nafion, for 30 min to improve the crystallinity of the polymeric structure of Nafion (Figure 1b).[31,32] During the thermal treatment, the residue in the airbrush was cleaned by spraying with the supplied IPA to the airbrush with high flow rates and pressure to the outside of

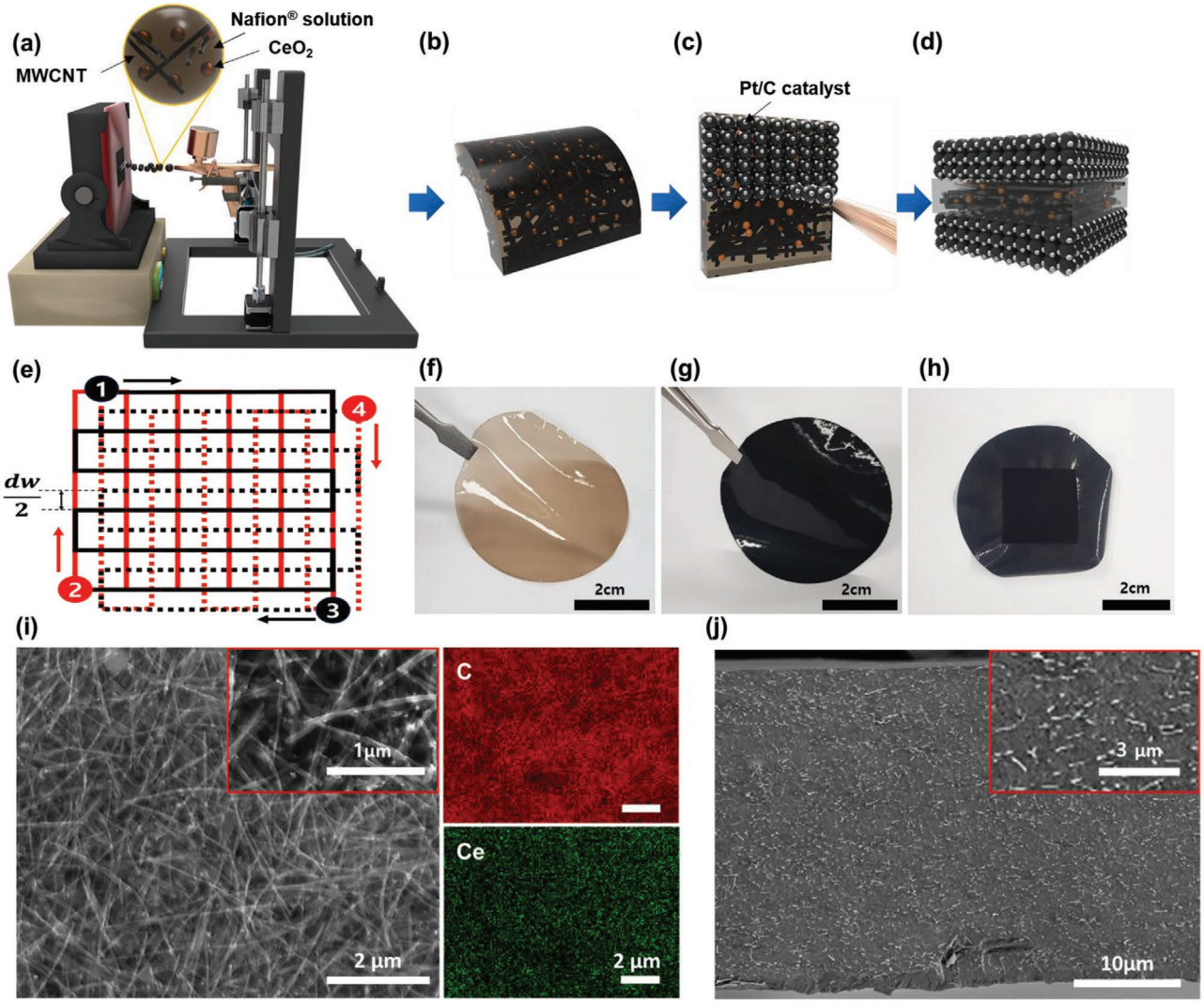

Figure 1. a–d) Schematic of MWCNTs/CeO_2-reinforced Nafion composite membrane and successive membrane electrode assembly (MEA) fabrication process by the spraying process. e) Designed serpentine spraying travel path. f) Digital images of prepared pure membrane, g) MWCNTs/CeO_2 composite membrane, and h) constructed MEA with composite membrane. SEM images of i) MWCNTs/CeO_2 layer without Nafion with normal view and with EDS elemental mapping images, and j) MWCNTs/CeO_2 composite Nafion membrane in cross-sectional view with the backscattered electrons (BSE) mode.

the membrane-coated substrate. Then, the catalyst deposition process for constructing the anode and the cathode was conducted by supplying the catalyst ink containing Pt/C and Nafion ionomer into the cleaned reservoir of the airbrush and spraying it onto each side of the fabricated membrane (Figure 1c,d). A thin metal mask with a square opening was placed on the membrane to deposit the desired amount of Pt catalyst on the target active area. When constructing the membrane and the catalyst layer, the spraying travel path was adjusted to have serpentine-like patterns with a 1-mm-sized interval length by modifying the G-code of the 3D printing system. To achieve the improved uniformity of the membrane and the catalyst layer, the center position of four each pattern was shifted to the half-width of the interval length, and the travel path direction was rotated by 90° after drawing every single serpentine pattern (Figure 1e). Figure 1f–h shows the images of the fabricated pure Nafion membrane (Figure 1f), MWCNTs/CeO_2-reinforced Nafion composite membrane (Figure 1g), and MEA with the reinforced membrane (Figure 1h) through the single spray-coating process. To employ MWCNTs and CeO_2, which effectively reinforce the polymeric membrane, proper dispersion and appropriate interfacial adhesion between the MWCNTs and polymeric Nafion matrix should be guaranteed. Generally, compared to conventional fillers, such as CeO_2 nanoparticles, heavily entangled MWCNTs having the morphological characteristic of the nanoscale diameter with a high aspect ratio suffer from considerable difficulties in the dispersion of the materials.[33] Thus, acid treatment with a mixture of sulfuric and nitric acids to pristine MWCNTs was performed to generate carboxylic groups on the carbon surface for better dispersibility.[34] Figure S1 (Supporting Information) shows the transmission electron microscopy (TEM) images of the CeO_2 nanoparticles.

We confirmed the average particle size of ≈25 nm and the elements of Ce and O are composed of atomic weight percent of 35.36 and 63.64, respectively. Figure S2 (Supporting Information) shows the XPS spectra of the MWCNTs with and without acid treatment. A significantly higher O1s peaks at 530.8 and 532.5 eV were observed in the case of acid-treated MWCNTs, which corresponds to C=O and C–O–H functional groups.[35] A solution of MWCNTs, CeO_2, and a mixture of 1-propanol and water without the Nafion ionomer was then sprayed onto the Si substrate while maintaining the same membrane fabrication condition, to examine the structural and compositional characteristics of MWCNTs and CeO_2 in the mixture. From the scanning electron microscopy (SEM) images of the MWCNTs/CeO_2 composite structure without Nafion and the corresponding energy-dispersive spectroscopy (EDS) mapping images of C and Ce (Figure 1i), it is confirmed that the MWCNTs and CeO_2 were well-dispersed and formed a uniform composite structure. Figure 1j shows the cross-sectional SEM image of the MWCNTs/CeO_2-reinforced Nafion composite membrane, and the agglomeration issue of the fillers was not observed over the entire membrane in the through-plane direction. The detailed analyses of the distribution of additional fillers in the composite membrane were performed by using an image analysis tool and additional SEM images with a backscattered detector (Figures S3 and S4, Supporting Information). This result can be obtained due to the advantage of the micro-droplet-based layer-by-layer deposition process via the spraying method, which can effectively avoid the bulk evaporation-driven self-assembly of the fillers in the polymeric matrix; generally, it is easily observed during the conventional casting-drying method (Figure S5, Supporting Information).[33,36]

2.2. Optimization of Membrane Fabrication Condition

Generally, it is challenging to manufacture a defect-free membrane with uniform thickness using the droplet-based deposition process of spray coating. To determine the optimal spraying condition, two important parameters of the nozzle-to-substrate distance (L = 30, 55, and 100 mm) and Nafion ionomer solution loading rates (Q = 0.35, 1.25, and 2.79 mL min^{-1}) were adjusted and fixed for each process. By considering the combination of multiple parameters, nine experimental cases were extensively and carefully examined. Other parameters, including the substrate temperature (85 °C), carrier gas pressure (1.5 bar), nozzle moving speed (60 mm s^{-1}), and Nafion ionomer concentration in solution (1 wt%), were fixed to be constant for all cases. Table S1 (Supporting Information) summarizes the experimental conditions. After fabricating the pure Nafion-sprayed membrane for each case, the surface morphological characteristics of membranes were observed using an optical microscope (**Figure 2**). The result of Case #5 demonstrates the most defectless smooth surface among the nine cases. For the other failed cases, as L decreases and Q increases, wave-like patterns on the surface significantly appear. However, as L increases and Q decreases, the surface bumps and agglomerated solid Nafion particles are generated on the membrane surface. The results can be interpreted in the aspect of the surface coverage of droplet spreading. When

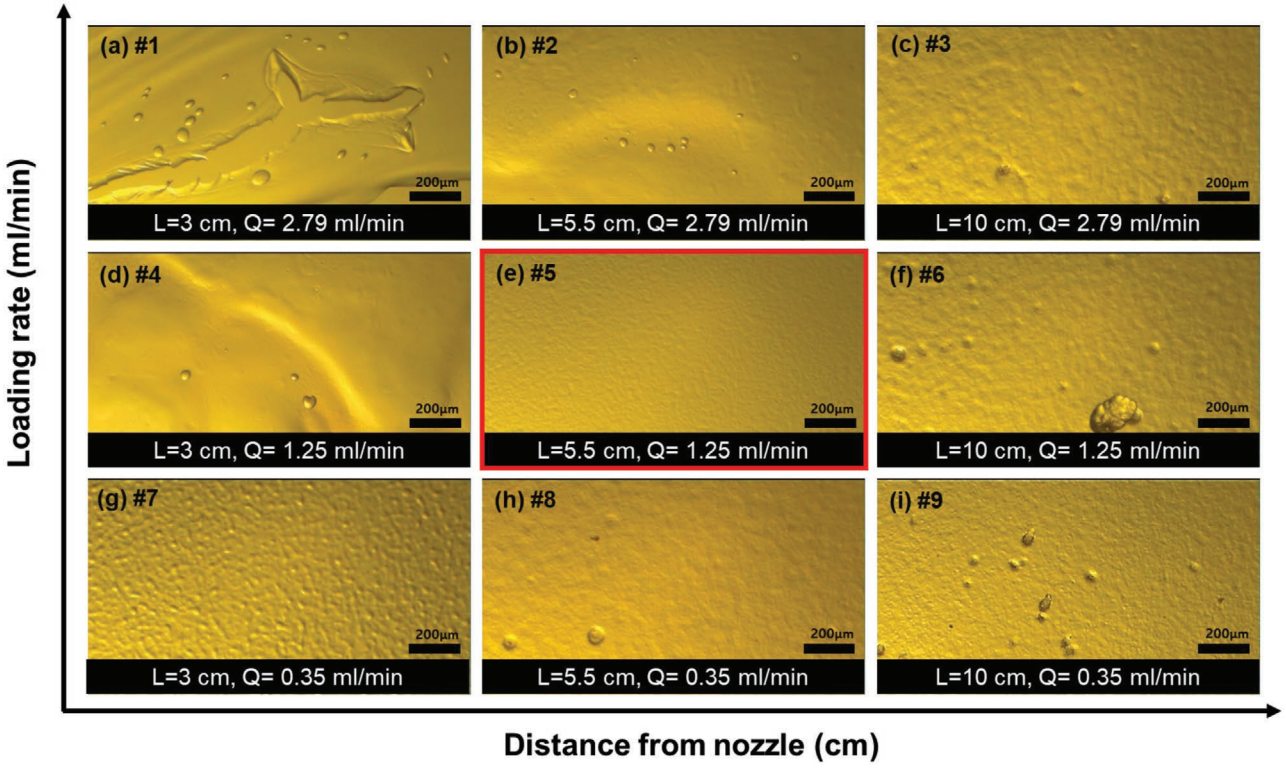

Figure 2. a–i) OM images for different surfaces of spray-based pure membranes by varying conditions of nozzle-to-substrate distance (*x*-axis) and solution loading rates (*y*-axis) (scale bar = 200 μm).

the surface of substrate was coated with excessive liquid droplets, the coffee-ring-like effect during the solvent evaporation resulted in the local flooding-induced accumulation of Nafion at the droplet edge, as in case #1. However, when the surface of the substrate was coated with insufficient liquid droplets, the scattered distribution of the Nafion formed bumps and agglomerates on the membrane surface, as in case #9. Furthermore, in this case, the solution can be evaporated along the long travel length, thus leaving solid powder on the surface.

To explain the optimal spray-coating condition for membrane fabrication, the simple model was set based on the surface coverage concept of the sprayed liquid droplet. The atomized liquid droplets of diameter D_0 are sprayed out from the nozzle, and the carrier gas with a velocity of V_0 delivers droplets to the substrate. The spherical droplets then spread out on the impacted substrate, which deforms the droplets to have a circular 2D thin sheet with diameter D_{max} on the surface. The relation between D_0 and D_{max} can be expressed in Equation (1).[37]

$$\frac{D_{max}}{D_0} = \sqrt{\frac{We+12}{3(1-\cos\theta)+4\left(We/\sqrt{Re}\right)}} \tag{1}$$

$$Re = \frac{\rho V_0 D_0}{\mu}, We = \frac{\rho {V_0}^2 D_0}{\sigma} \tag{2}$$

where μ is the viscosity of the liquid, ρ is the density of the liquid, σ is the surface tension of the solution, and θ is the contact angle of a droplet on the substrate. To develop the defect-free membrane through the spray-coating method, the overall sprayed droplets from the nozzle with a volume of U should completely cover the spray-spot area with a diameter D_s on the substrate; within the time that the spray nozzle moves to the next spot with a moving speed of V_n. The duration time τ for spraying on a unit spot area and U can then be expressed as follows (Equations (3)–(4)).

$$\tau = \frac{D_s}{V_n} \tag{3}$$

$$U = Q \cdot \tau = n\frac{4}{3}\pi {D_0}^3 \tag{4}$$

Based on the assumption that all droplets with an initial diameter of D_0 are uniformly sprayed out from the nozzle, the number of droplets n is determined as follows.

$$n = \frac{Q \cdot \tau}{\frac{4}{3}\pi {D_0}^3} \tag{5}$$

Finally, the coverage indicator k, defined as the total surface coverage of the sprayed droplet during the time divided by the area of a single spot, was set as Equation (6).

$$k = \frac{n\left(\frac{\pi}{4}{D_{max}}^2\right)}{\frac{\pi}{4}{D_s}^2} = n\left(\frac{D_{max}}{D_s}\right)^2 \tag{6}$$

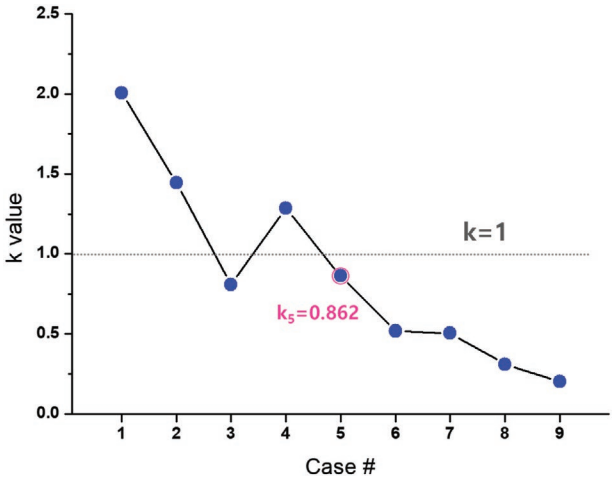

Figure 3. Plot of coverage indicator (k) for nine experimental cases.

The value of $k = 1$ means that the substrate's surface would be completely covered with the impacted droplet solution without an overlapped region, thus assuming a uniform distribution of the droplet. To determine the k value for each case, the θ value of the solution on the substrate and the droplet-traveling velocity (V_0) at the substrate's position from the nozzle (L = 30, 55, and 100 mm) was determined. The θ value was measured as ≈5° (Figure S6, Supporting Information), and the measured V_0 was inversely proportional to L and interestingly independent of Q. The values of V_0 were measured as 31.2, 20.4, and 10.6 m s^{-1} at L values of 30, 55, and 100 mm, respectively. Moreover, the initially atomized droplet size (D_0) was estimated as ≈11.9 ± 2.6 µm from observing the D_{max} value on the surface after the spraying whose values are similar to those in previously reported studies using an airbrush.[38] Moreover, the pure Nafion and MWCNTs/CeO_2/Nafion solutions show comparable D_0 ranges (Figure S7, Supporting Information). **Figure 3** shows the calculated k values for the nine experimental cases where case #5 exhibits k = 0.862, which is the closest to 1 among all cases. Furthermore, this result agrees with the experimental results in Figure 2. For case #1 with high Q and short L, k = 2.00, indicating that the excessive coverage of the liquid droplets compared to the spot area would generate wave-like patterns on the membrane. Furthermore, for case #9 with low Q and long L, k = 0.203, indicating that liquid droplets would not sufficiently cover the complete spot area, resulting in surface bumps and agglomerated solid Nafion particles. Although k is not the only factor to be considered when manufacturing the membrane by spray coating, this analysis agrees with the observed experimental results. Based on these results, all membranes, including the sprayed pure Nafion and the MWCNTs/CeO_2 composite Nafion membranes, were fabricated under the process condition of case #5.

2.3. Characterization of Prepared Membranes

Compared to the commercial Nafion 211 membrane (N211), to examine and compare the mechanical properties of the prepared spray-based membranes, uniaxial tensile tests for each

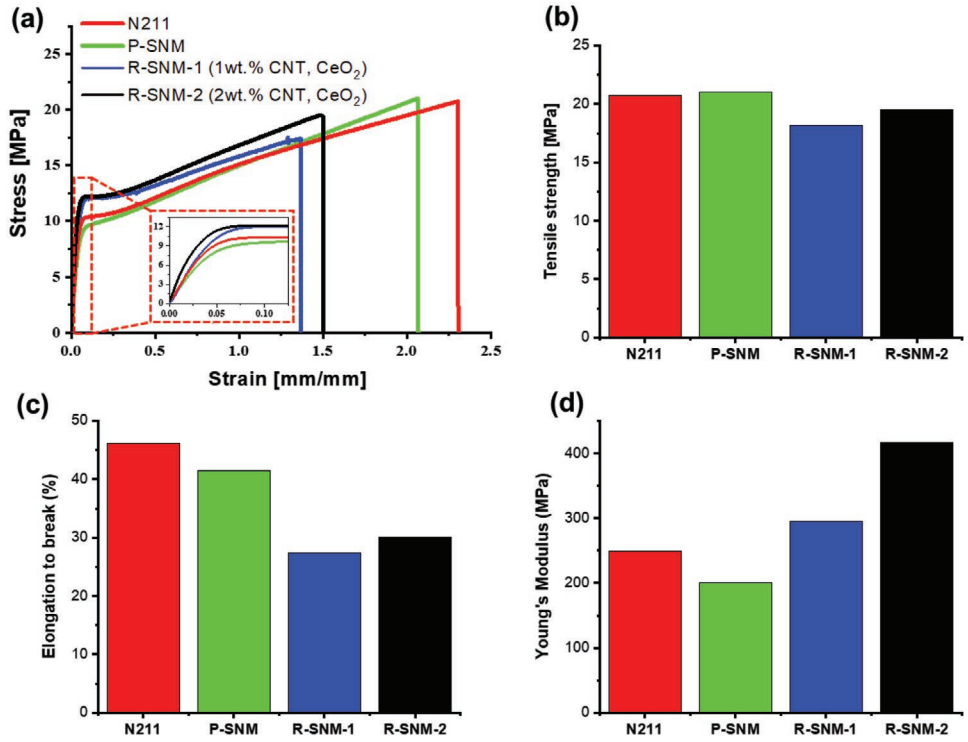

Figure 4. Mechanical strength properties of prepared membranes, including Nafion 211, pure-sprayed Nafion, and composite membranes with 1 wt% MWCNTs/CeO_2 (R-SNM-1) and 2 wt% MWCNTs/CeO_2 (R-SNM-2): a) stress–strain curves, b) tensile strength, c) elongation at break, and d) Young's modulus.

membrane were performed. The thickness of all spray-based membranes were set in a range of 26–27 µm, which is the same as that of the commercial membrane. **Figure 4** shows the stress–strain curves of the membranes with a pure-sprayed Nafion membrane (P-SNM), reinforced sprayed Nafion membranes with each x wt% loading amount of MWCNTs and CeO_2 (R-SNM-x, x = 1 and 2), and N211. The detailed composition ratios of MWCNTs, CeO_2, and Nafion ionomer for the samples are summarized in Table S2 (Supporting Information). Figure 4b–d shows the values of the tensile strength, elongation at break, and Young's modulus of these prepared membranes, respectively. For the R-SNM-2 case, the membrane exhibited >67% higher Young's modulus (416.9 MPa) than the reference N211 membrane (249.7 MPa), indicating that R-SNM-2 has considerably high stiffness that resists mechanical deformation under the applied external load, as shown in Figure 4d and the magnified inset image of Figure 4a. Moreover, despite a shortened elongation at break of R-SNM-2, it shows a comparable tensile strength to that of the N211 membrane. The origin of the superior mechanical properties of R-SNM-2 compared to other membranes, including R-SNM-1, can be explained by taking advantage of the excellent mechanical properties of the inserted MWCNTs.[23,24] Moreover, the additional characterization of membrane properties, including proton conductivity, dimensional stability, and water uptake, which significantly affect the stability and performance of the PEMFC, was performed (**Table 1**). The R-SNM-2 membrane shows a marginally reduced proton conductivity by ≈4.6% compared to the commercial N211, although a total of 4 wt% of MWCNTs and CeO_2 fillers are incorporated in the Nafion matrix. This indicates that the inserted fillers were uniformly dispersed without considerable agglomeration with the aid of the layer-by-layer spray-coating and the acid treatment of MWCNTs. Figure S8 shows the experimental apparatus for measuring the membrane conductivity, and the experimental details are provided in the Experimental Section. Moreover, the in-plane dimensional stability is improved because of the stacked MWCNTs. Interestingly, the amount of water uptake of the spray-based Nafion membranes increases, which is attributed to the use of low equivalent weight (EW) Nafion ionomer of 1000 (EW of

Table 1. Properties of prepared membranes.

Samples	Ion conductivity at 70 °C [S cm^{-1}]	Dimensional stability (x-axis) [%]	Dimensional stability (y-axis) [%]	Dimensional stability (z-axis) [%]	Water uptake [%]
N211	0.2484	12.5	15	24	28.87
P-SNM	0.2410	13.75	12.82	25.93	37.37
R-SNM- 2	0.2370	12.5	12.5	27.59	36

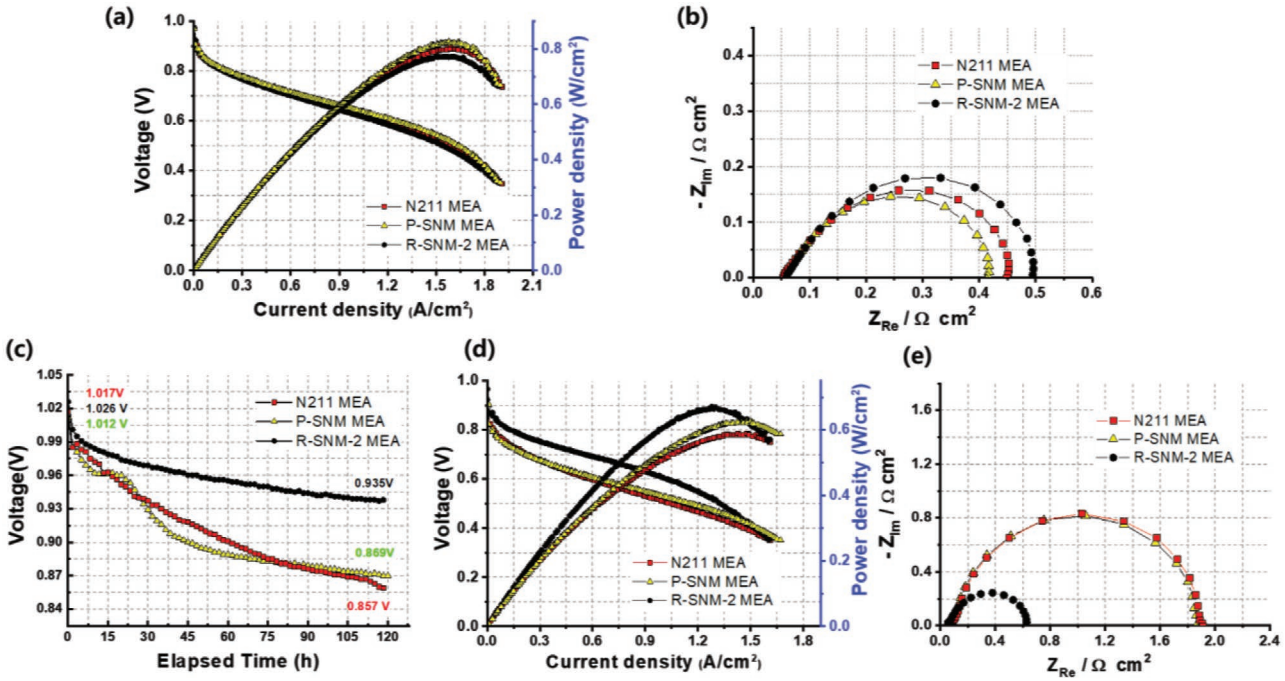

Figure 5. a) Polarization curves under 92% RH at 70 °C with H_2/Air flow rate = 300/1000 mL min^{-1}. b) Corresponding EIS spectra at 0.8 V. c) OCV decay spectra over 120 h testing under accelerated conditions. d) Polarization curves under 92% RH at 70 °C with H_2/Air flow rate = 300/1000 mL min^{-1}) after OCV test. e) Corresponding EIS spectra at 0.8 V after OCV test.

N211 = 1100). Additionally, hygroscopic and hydrophilic properties of CeO_2 and acid-treated MWCNTs can be helpful to retain water molecules more effectively.[39]

2.4. Electrochemical Performance and Durability

Next, to evaluate the performance and durability of MEAs with prepared membranes, individual cells were constructed, and electrochemical performance was measured. **Figure 5**a shows the polarization curves of prepared MEAs under the operating condition of 92% relative humidity (RH) at 70 °C with H_2/air flow rate of 300/1000 mL min^{-1} without backpressure. Among MEAs, P-SNM MEA shows the highest maximum power density of 826 mW cm^{-2}, which exceeds that of the commercial membrane of N211 (803 mW cm^{-2}) with the same thickness. This result indicates that the spraying condition for manufacturing the membrane is well optimized. For the MEA with R-SNM-2, it exhibits a little lower performance of 774 mW cm^{-2} because of the insertion of non-proton conductive fillers of MWCNTs and CeO_2 which increased ohmic resistance. The EIS measurement (Figure 5b) demonstrated that higher ohmic resistance was observed in the MEA with R-SNM-2. However, the increased ohmic resistance ratio is only 6.5% compared to the MEA with P-SNM, which indicates that the fillers were uniformly distributed to minimize the proton transport blockage. After confirming the comparable initial performance of the MEA with R-SNM-2 compared to the commercial membrane, to verify the long-term durability of the PEMFC fabricated by the single spray-coating process, the open-circuit voltage (OCV) test, a representative chemical durability evaluation protocol, was conducted.[29] For the OCV test, the cell temperature was maintained at 90 °C and 30% RH, which condition is for supplying partially humidified H_2 (300 mL min^{-1}) and O_2 (300 mL min^{-1}). For this test, the OCV decay rate is used as an indicator of the membrane chemical degradation rate from an attack of generated hydroxyl (HO•) and hydroperoxyl (HOO•) radical species, and the radical scavenging effect of CeO_2 in the composite membrane is described in Figure S9 (Supporting Information).[14,29] As shown in Figure 5c, R-SNM-2 shows a significantly low decay rate of 0.758 mV h^{-1} than that of the MEAs with N211 membrane (1.333 mV h^{-1}) and P-SNM membrane (1.191 mV h^{-1}) because of the insertion of CeO_2 nanoparticles, which act as an effective radical scavenger. Figure 5d,e shows the polarization curves and the corresponding EIS spectra for the MEAs after OCV tests for 120 h under the operating condition of 92% RH at 70 °C with H_2/Air flow rate of 300/1000 mL min^{-1} without backpressure. Note that the MEA with R-SNM-2 shows an almost recovered OCV value of 0.966 V compared to its initial value of 0.974 V before the OCV test. However, the MEA with commercial N211 membrane shows an OCV value of 0.868 V, which is over 10% reduced value than the initial OCV value (0.972 V), which indicates that the membrane underwent permanent degradation. In terms of performance, the MEA with R-SNM-2 shows a slightly reduced performance (1.02 A cm^{-2} at 0.6 V) with a reduction of ≈8.93% after the OCV test; however, the MEA with commercial N211 shows significantly reduced performance (0.58 A cm^{-2} at 0.6 V), which is over 50% loss compared to its initial value. Interestingly, for MEAs with N211 and P-SNM, the maximum power densities appeared at 0.4 V, which value is shifted much higher overpotential region compared to that of 0.5 V before the OCV

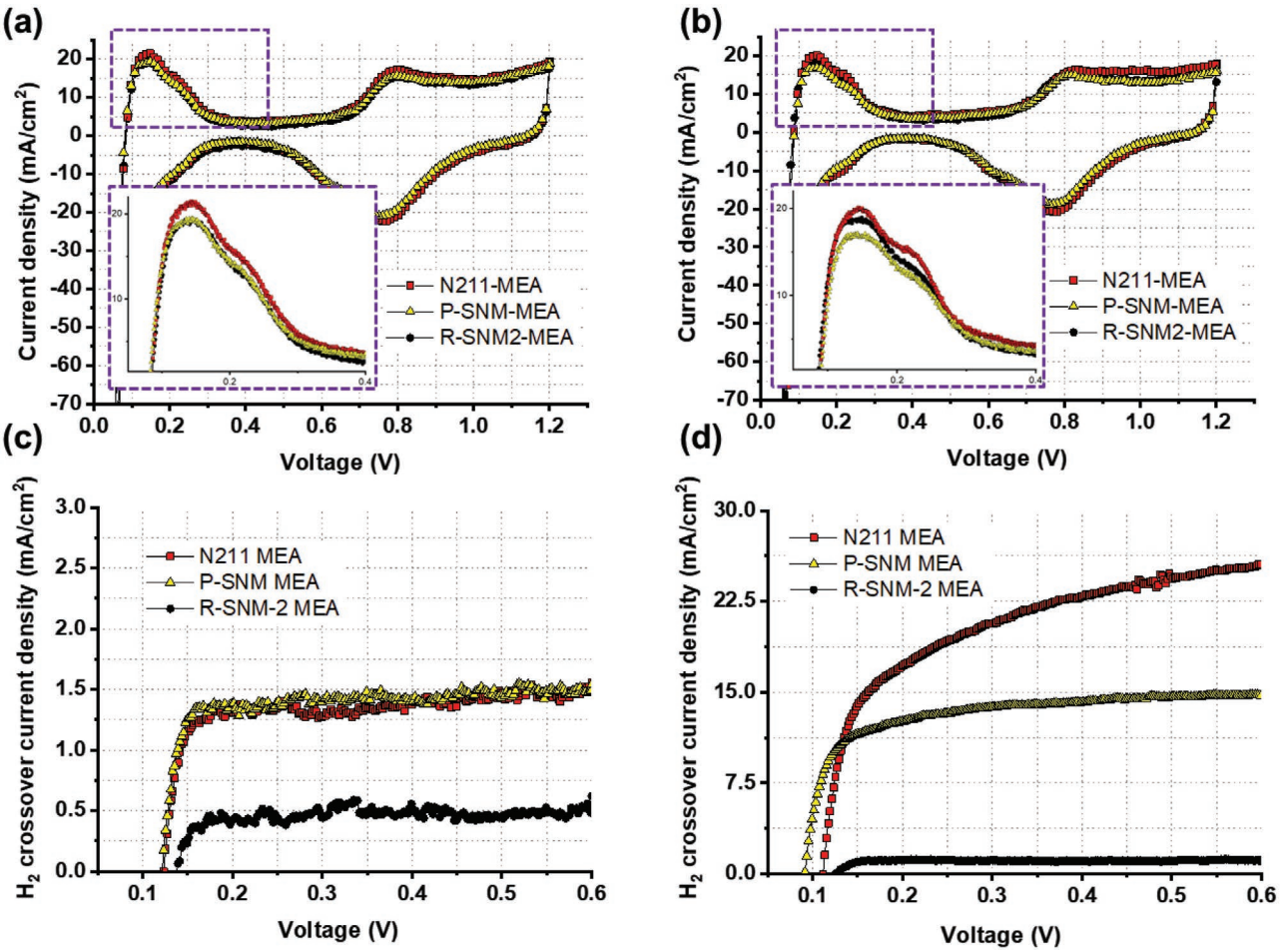

Figure 6. Cyclic voltammetry (CV) spectra under 100% RH at 70 °C with H_2/N_2 flow rate = 50/200 mL min^{-1} a) before and b) after OCV test. Linear sweep voltammetry (LSV) spectra under 100% RH at 70 °C with H_2/N_2 flow rate = 200/200 mL min^{-1} c) before and d) after OCV test.

test. Such a trend indicates that, after the OCV test, the mass transport of the generated water and oxygen at the cathode was improved for the samples. Because the generated radicals can oxidize the carbon support of the electrode and the membrane,[40] this result can be considered as the degradation of the catalyst-driven change of the porosity of the cathode. Moreover, this result is related to the reduction of the electrochemically active surface area (ECSA).

Figure 6a,b shows the cyclic voltammetry (CV) spectra before and after OCV tests. The ECSA can be obtained from the hydrogen adsorption/desorption range in each CV curve, as shown in the magnified inset images. For the MEA with R-SNM-2, the ECSA value reduced by ≈2.97% after the OCV tests; however, the MEAs with N211 and P-SNM show significantly reduced ECSA by ≈11.49% and 16.40%, respectively. This result confirms that adding CeO_2 into the membrane can increase the durability of the membrane and the electrode, i.e., improve the MEA's overall stability. Furthermore, as an important factor for membrane stability, the extent of hydrogen crossover for each MEA was measured before and after OCV tests. Figure 6c shows the linear sweep voltammetry (LSV) spectra before the OCV test at 100% RH and 70 °C with H_2 and N_2 supply to the anode and cathode at flow rates of 200 mL min^{-1}, respectively. MEA with R-SNM-2 shows an extremely low hydrogen crossover current density of 0.5 mA cm^{-2} at 0.4 V, which is 65% less than that of the MEAs with N211 and P-SNM. The hydrogen crossover flux is calculated from the measured current densities and Faraday's law,[41]

$$J_{\mathrm{H_2\ crossover\ flux}} = \frac{j_{\mathrm{current\ density}}}{n\,\mathrm{F}} \tag{7}$$

where n is the number of electrons taking part in the hydrogen oxidation reaction (n = 2) and F is the Faraday constant (96 485 C mol^{-1}). The hydrogen crossover flux values of MEAs with R-SNM-2, P-SNM, and N211 are 2.59×10^{-9}, 7.26×10^{-9}, and 7.31×10^{-9} mol cm^{-2} s, respectively. This result confirms that the insertion of MWCNTs and CeO_2 with uniform stacking by the layer-by-layer spray coating method can effectively reduce hydrogen crossover while avoiding the electric crossover through the membrane, even with the use of conductive MWCNTs. After OCV tests, a remarkable hydrogen crossover increment is observed for the MEAs with the N211 and P-SNM membranes, indicating that the defect (i.e., pinhole) is generated on membranes and permanent degradation occurred during the OCV test or the membrane gets thinned because of

Table 2. Summary of the measured electrochemical properties of the prepared MEAs before and after OCV test.

Samples	OCV [V]	Maximum power density [W cm^{-2}]	Current density at 0.6 V [A cm^{-2}]	R_{ohm} [Ω cm^2] at 0.8 V	$R_{LF\text{-}HF}$ [Ω cm^2] at 0.8 V	H_2 crossover current density [mA cm^{-2}]	ECSA [m^2 g_{pt}^{-1}]
Before OCV test							
N211 MEA	0.972	0.803	1.17	0.0543	0.396	1.41	60.9
P-SNM MEA	0.970	0.826	1.24	0.0551	0.359	1.40	56.7
R-SNM-2 MEA	0.974	0.774	1.12	0.0587	0.435	0.50	57.3
After OCV test							
N211 MEA	0.868 (–10.70%)	0.589 (–26.65%)	0.58 (–50.43%)	0.0531 (–2.21%)	1.853 (+368%)	22.9 (+1524%)	53.9 (–11.49%)
P-SNM MEA	0.905 (–6.70%)	0.626 (–24.21%)	0.639 (–48.47%)	0.0535 (–2.90%)	1.821 (+407%)	14.2 (+914%)	47.4 (–16.40%)
R-SNM-2 MEA	0.966 (–0.82%)	0.671 (–13.31%)	1.02 (–8.93%)	0.0559 (–4.77%)	0.569(+30.8%)	1.04 (+108%)	55.6 (–2.97%)

material loss from the radical attack (Figure 6d). However, the MEA with R-SNM-2 shows a marginally increased hydrogen crossover flux of 5.39×10^{-9} mol cm^{-2} s, which is sufficiently low and even lower than the values of other MEAs before the OCV test. This result agrees with the results of OCV test (Figure 6c) and explains the instant OCV recovery of the MEA during the polarization test (Figure 6d). All the measured electrochemical results are summarized in **Table 2**.

Figure 7a–c shows the cross-sectional images of the prepared membranes of N211 (Figure 7a), P-SNM (Figure 7b), and R-SNM-2 (Figure 7c) before electrochemical measurements, indicating that all membranes have almost the same initial thickness. However, after the OCV test, the membrane thickness was considerably thinned for the N211 (Figure 7d) and P-SNM (Figure 7e) cases, which agrees with the results of the dramatic hydrogen crossover increment and significant performance reduction of MEAs with such membranes after the OCV test. For the R-SNM-2, the membrane thickness was almost unchanged (Figure 7f), and the existence of CeO_2 after the OCV test was confirmed by the EDS elemental mapping image (Figure 7g). Furthermore, fluorine concentration in the drain water during the OCV tests at every 24 h at the anode and cathode was confirmed because the fluorine concentration indicates the degradation of the PFSA-based Nafion membrane (Figure 7h,i).[19] Although the cases MEAs with N211 and P-SNM show increased fluorine concentration as the OCV test progress, the case of MEA with R-SNM-2 shows an almost constant and remarkably low fluorine concentration than that of other MEAs. This trend obviously demonstrates the high durability of the R-SNM-2 membrane. Finally, to investigate the appropriate loading amount of the fillers, additional characterization for MEA with the reinforced membranes with different MWCNTs and CeO_2 loading amounts (R-SNM-1 and R-SNM-3), including polarization tests and EIS measurements (Figure S10, Supporting Information), LSV for hydrogen crossover (Figure S11, Supporting Information), CV spectra (Figure S12, Supporting Information), OCV test for 24 h (Figure S13, Supporting Information), and fluorine concentration measurements in the drain water during the OCV test (Figure S14, Supporting Information) were conducted. The results are summarized in Table S3 (Supporting Information). Based on these results, the excessive loading amount of MWCNTs and CeO_2 (R-SNM-3) can induce considerable performance loss because of the primarily increased ohmic resistance, whereas the deficient loading amount of MWCNTs and CeO_2 (R-SNM-1) limits the increment in mechanical properties (Figure 4a) and chemical durability (Figures S13 and S14, Supporting Information) of the membrane. Therefore, introducing the proper amount of fillers into the membranes is critical, in addition to the optimization of the membrane fabrication process via spray coating.

3. Conclusion

Herein, a simplified manufacturing process for developing a highly durable MEA using the single spray-coating method was proposed. To achieve a defect-free and robust membrane with uniform thickness, the optimized spray-coating condition was investigated by fabricating membranes with varying deposition conditions, such as nozzle-to-substrate distance and solution-loading rate. And the experimental results are validated with a simple theoretical model based on the concept of surface coverage of the sprayed liquid droplet. The results revealed that optimal conditions for the membrane fabrication by avoiding excessive liquid droplets induced wave-like patterns on the surface, and surface bumps and agglomerated solid Nafion particles because of insufficiently coated liquid droplets on the spot. Furthermore, by adding acid-treated MWCNTs and CeO_2 into the Nafion ionomer solution and depositing it through layer-by-layer spray coating, a mechanically and chemically durable reinforced Nafion composite membrane was obtained without the issues of agglomeration and protrusion of fillers. Despite using additional fillers of a total 4 wt% in the Nafion matrix, MWCNTs/CeO_2-reinforced Nafion composite membrane showed considerably improved mechanical properties because of the excellent mechanical properties of MWCNTs while minimizing the loss of proton conductivity. After constructing MEAs with the commercial Nafion 211, pure-sprayed Nafion, and reinforced composite Nafion membranes using the same single spray-coating method, electrochemical polarization and OCV durability tests were performed. MEA with the reinforced composite Nafion membrane showed significantly improved PEMFC durability while securing comparable initial performance and considerably higher performance after the durability test. We believe that this novel methodological approach for the well-optimized single spray-coating method can contribute to advances in commercializing PEMFCs into the market by simplifying the MEA fabrication process and increasing the lifetime of PEMFCs.

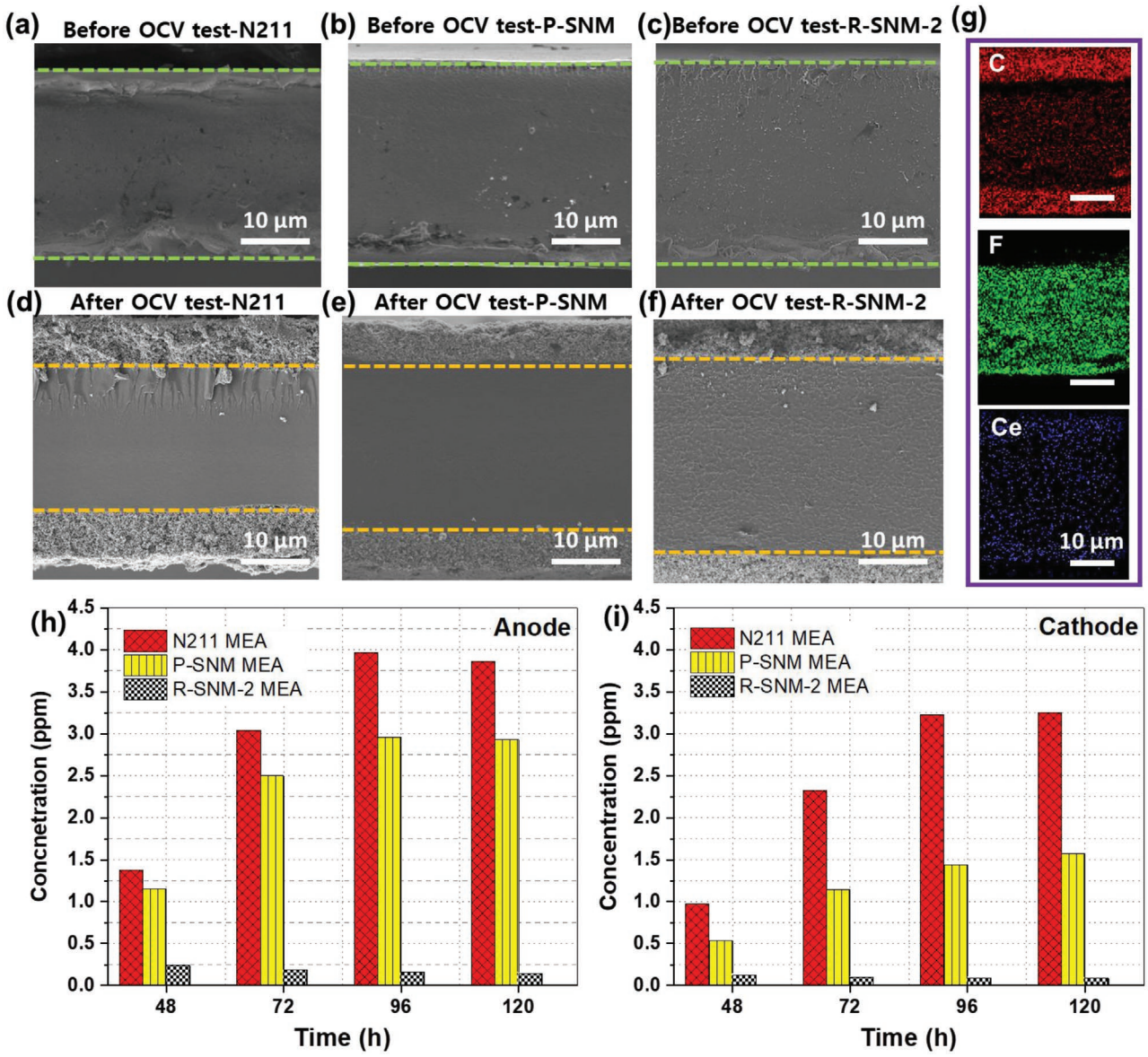

Figure 7. Cross-sectional SEM images for a–c) prepared membranes before OCV test and d–f) for MEAs with such membrane after OCV test. g) EDS elemental mapping images for MEA with reinforced membrane (R-SNM2-MEA) after OCV test. Fluorine concentration in drain water during OCV tests at every 24 h at h) anode and i) cathode sides.

4. Experimental Section

Preparation of MWCNTs/CeO_2/Nafion Solution: Nafion solution of 5 wt% amount (Chemours, D520 Nafion solution, EW 1000) was diluted to 1 wt% with deionized (DI) water, 1-propanol, and ethanol at a weight ratio of 45:48.5:1.5 for spraying by reducing the solution's viscosity. Next, the acid-treated MWCNTs (Sigma Aldrich, 50–90 nm diameter) were dispersed in the diluted Nafion solution by varying the weight ratio of 1%, 2%, and 3% compared to the solid Nafion content. Acid treatment was performed following the method of previously reported paper using a mixture of sulfuric (95%, Samchun chemical) and nitric (70%, Samchun chemical) acids with a volume ratio of 3:1 at 80 °C for 12 h.[34] Next, the radical scavenger, CeO_2 (Sigma Aldrich, ≈25-nm size), was added to the MWCNTs/Nafion solution with the same weight ratio of MWCNTs and uniformly dispersed with ultrasonication for 1 h.

MEA Fabrication via Single Spray-Coating System: MWCNTs/CeO_2-reinforced Nafion composite and pure Nafion membranes were fabricated using the lab-made single spraying-coating device by integrating the air brush (nozzle size of 0.7 mm, GP-70, Bettle Bug Inc.) into a commercial 3D printing machine (Ender-3, Creality 3D) using a spray handle jig. The prepared mixture of Nafion solution with MWCNTs and CeO_2 was sprayed onto the Si wafer substrate mounted on the hotplate at 85 °C with the optimized spraying condition of the solution-loading rate of 1.25 mL min^{-1} and nozzle-to-substrate distance of 5.5 cm. The spray travel path comprised four serpentine-like patterns with a total size of 5.9 × 5.9 cm^2 and a 1-mm interval length. In each pattern, the center position was shifted by 0.5 mm, and the travel path was rotated by 90° after drawing every single serpentine pattern. For comparison, pure-sprayed Nafion membrane was prepared using the Nafion solution without fillers, and a commercial Nafion membrane (NR-211, 25–27 μm thickness, Dupont) was purchased. After the membrane deposition process, the membrane-coated substrate was thermally annealed on the same hotplate at 120 °C for 30 min. During thermal annealing, air brush was cleaned using an IPA solution. Furthermore, one side of the catalyst

layer was deposited by spraying the catalyst ink composed of Pt on carbon powder (46.6 wt% Pt, Tanaka), Nafion ionomer solution (5 wt%, Sigma Aldrich), IPA, and deionized water. For constructing the other side of catalyst layer, the membrane coated with a one-side electrode was detached from the substrate and the backside was attached to the substrate, followed by spraying the catalyst ink. During the catalyst layer deposition using the same spray coating device, the active area was set to 5 cm^2 (2.23×2.23 cm^2) using the metal mask with a square opening, and the size of the spray travel path was adjusted to the active area. The Pt-loading amount for both anode and cathode was 0.2 mg_{pt} cm^{-2} for all MEAs.

Characterizations: TEM images of the commercial CeO_2 nanoparticles were obtained using an FEI TITAN 80-300 transmission electron microscope operated at 200 kV. The characteristics of acid-treated MWCNTs were investigated using the field-emission SEM (FE-SEM) (HITACHI, SU-5000) and an X-ray photoelectron spectrometer (XPS) (Sigma Probe, Thermo Fisher Scientific) using AlKα as the X-ray source. The cross-sectional SEM images of MEAs before and after the OCV test were obtained by freezing and fracturing MEAs with liquid nitrogen. The stress-strain curves of prepared membranes were then measured at room temperature using a universal test machine (3340, Instron Corp, USA) with a strain rate of 5 mm min^{-1} and a sample size of 1×2 cm^2 (width and length). The proton conductivity of membranes was measured using a four-electrode conductivity cell (Figure S6, Supporting Information). The membranes were cut to 1×4 cm^2, and then inserted into the conductivity cell with four Pt wire electrodes at a distance of 1 cm for each electrode (four-probe method). The membrane resistance was obtained by EIS measurement in the frequency range from 1 MHz to 1 Hz at a constant current of 0.1 mA at 70 °C by supplying completely humidified nitrogen gas to the cell. The in-plane conductivities of membranes were calculated based on the measured resistance (Equation (8)).[42]

$$\sigma = \frac{L}{RA} \tag{8}$$

where L is the distance between the two electrodes (cm), R is the membrane resistance (Ω), and A is the cross-sectional area of the membrane (cm^2). The dimensional stability and water uptake properties of membranes were determined as follows.

$$\%\ \text{Length change} = 100\left(\frac{L_f - L_i}{L_i}\right) \tag{9}$$

$$\%\ \text{Thickness change} = 100\left(\frac{t_f - t_i}{t_i}\right) \tag{10}$$

$$\%\ \text{Water uptake} = 100\left(\frac{m_f - m_i}{m_i}\right) \tag{11}$$

The initial dimension and mass of prepared membranes were obtained after drying them in an oven at 80 °C for 12 h. Next, to calculate the changed values of dimension and mass, the membranes were completely hydrated in DI water at 60 °C for 12 h.

Electrochemical Measurements: The polarization curves for prepared MEAs were obtained using a fuel cell test station (CNL, Korea) via the current sweep method with increments of 5 mA cm^{-2} until the voltage reaches 0.35 V. The same operating condition was maintained for all MEAs under 92% RH at 70 °C. Moreover, under the same conditions, the EIS spectra were measured by the impedance analyzer (HCP-803, Biologic) at 0.8 V with an amplitude of 10 mV in the frequency range of 15 kHz to 0.1 Hz. To determine the ECSA, CV was conducted at 70 °C by supplying completely humidified H_2 (50 mL min^{-1}) and N_2 (200 mL min^{-1}) to the anode (counter and reference electrodes) and the cathode (working electrode). For the hydrogen crossover measurement, LSV was conducted under the same measurement conditions of the CV, but with a different H_2 flow rate (200 mL min^{-1}). For the OCV test, the reactant gases of H_2/O_2 (300/300 mL min^{-1}) were supplied to the cell under 30% RH at 90 °C, and OCV values were constantly recorded for 120 h. During this test, the drain water from the anode and cathode was collected at 48, 72, 96, and 120 h to measure fluorine concentration changes. Each drain water was mixed with the same amount of TISAB (total ionic strength adjuster buffer) solution and Fluorine concentration was measured using the calibrated fluoride ion-selective electrode (A214, Thermo Scientific).

Supporting Information

Supporting Information is available from the Wiley Online Library or from the author.

Acknowledgements

E.C. and S.M.K. contributed equally to this work. This work was funded by the National Research Foundation of Korea (NRF) grant (No. 2019R1C1C1004462) and Korea Electric Power Corporation (Grant No. R21XO01-27).

Conflict of Interest

The authors declare no conflict of interest.

Data Availability Statement

The data that support the findings of this study are available from the corresponding author upon reasonable request.

Keywords

spray, membrane electrode assembly (MEA), reinforced membrane, fuel cells, radical attack, durability

Received: October 16, 2021
Revised: February 15, 2022
Published online:

[1] S. Y. Lim, S. Martin, G. Gao, Y. Dou, S. B. Simonsen, J. O. Jensen, Q. Li, K. Norrman, S. Jing, W. Zhang, *Adv. Funct. Mater.* **2021**, *31*, 2006771
[2] K. Kodama, T. Nagai, A. Kuwaki, R. Jinnouchi, Y. Morimoto, *Nat. Nanotechnol.* **2021**, *16*, 140.
[3] H. L. Nguyen, J. Han, X. L. Nguyen, S. Yu, Y.-M. Goo, D. D. Le, *Energies* **2021**, *14*, 4048.
[4] T. Suzuki, S. Tsushima, S. Hirai, *Int. J. Hydrogen Energy* **2011**, *36*, 12361.
[5] M. Breitwieser, T. Bayer, A. Büchler, R. Zengerle, S. M. Lyth, S. Thiele, *J. Power Sources* **2017**, *351*, 145.
[6] M. Klingele, B. Britton, M. Breitwieser, S. Vierrath, R. Zengerle, S. Holdcroft, S. Thiele, *Electrochem. Commun.* **2016**, *70*, 65.
[7] M. Breitwieser, C. Klose, A. Hartmann, A. Büchler, M. Klingele, S. Vierrath, R. Zengerle, S. Thiele, *Adv. Energy Mater.* **2017**, *7*, 1602100.
[8] M. Breitwieser, C. Klose, M. Klingele, A. Hartmann, J. Erben, H. Cho, J. Kerres, R. Zengerle, S. Thiele, *J. Power Sources* **2017**, *337*, 137.

[9] T. Bayer, H. C. Pham, K. Sasaki, S. M. Lyth, *J. Power Sources* **2016**, *327*, 319.
[10] M. Klingele, M. Breitwieser, R. Zengerle, S. Thiele, *J. Mater. Chem. A* **2015**, *3*, 11239.
[11] A. Kusoglu, A. Z. Weber, *Chem. Rev.* **2017**, *117*, 987.
[12] M. Zatoń, J. Rozière, D. J. Jones, *Sustainable Energy Fuels* **2017**, *1*, 409.
[13] N. S. Khattra, A. M. Karlsson, M. H. Santare, P. Walsh, F. C. Busby, *J. Power Sources* **2012**, *214*, 365.
[14] K. R. Yoon, K. A. Lee, S. Jo, S. H. Yook, K. Y. Lee, I. D. Kim, J. Y. Kim, *Adv. Funct. Mater.* **2019**, *29*, 1806929.
[15] S. Jo, K. R. Yoon, Y. Lim, T. Kwon, Y. S. Kang, H. Sohn, S. H. Choi, H. J. Son, S. H. Kwon, S. G. Lee, S. S. Jang, S. Y. Lee, H. J. Kim, J. Y. Kim, *Small Methods* **2021**, *5*, 2100285.
[16] C. Klose, M. Breitwieser, S. Vierrath, M. Klingele, H. Cho, A. Büchler, J. Kerres, S. Thiele, *J. Power Sources* **2017**, *361*, 237.
[17] C. Lee, J. Park, Y. Jeon, J. I. Park, H. Einaga, Y. B. Truong, I. L. Kyratzis, I. Mochida, J. Choi, Y. G. Shul, *Energy Fuels* **2017**, *31*, 7645.
[18] Z. Jie, T. Haolin, P. Mu, *J. Membr. Sci.* **2008**, *312*, 41.
[19] S. Lee, W. Jang, M. Kim, J. E. Shin, H. B. Park, N. Jung, D. Whang, *Small* **2019**, *15*, 1903705.
[20] L. Cao, H. Wu, P. Yang, X. He, J. Li, Y. Li, M. Xu, M. Qiu, Z. Jiang, *Adv. Funct. Mater.* **2018**, *28*, 1804944.
[21] J. Zhang, G. Jiang, M. Goledzinowski, F. J. E. Comeau, K. Li, T. Cumberland, J. Lenos, P. Xu, M. Li, A. Yu, Z. Chen, *Small Methods* **2017**, *1*, 1700237.
[22] A. Iwan, M. Malinowski, G. Pasciak, *Renewable Sustainable Energy Rev.* **2015**, *49*, 954.
[23] G. He, J. Zhao, S. Hu, L. Li, Z. Li, Y. Li, Z. Li, H. Wu, X. Yang, Z. Jiang, *ACS Appl. Mater. Interfaces* **2014**, *6*, 15291.
[24] N. J. Steffy, V. Parthiban, A. K. Sahu, *J. Membr. Sci.* **2018**, *563*, 65.
[25] A. M. Baker, L. Wang, W. B. Johnson, A. K. Prasad, S. G. Advani, *J. Phys. Chem. C* **2014**, *118*, 26796.
[26] L. Wang, D. M. Xing, H. M. Zhang, H. M. Yu, Y. H. Liu, B. L. Yi, *J. Power Sources* **2008**, *176*, 270.
[27] A. M. Baker, L. Wang, S. G. Advani, A. K. Prasad, *J. Mater. Chem.* **2012**, *22*, 14008.
[28] B. P. Pearman, N. Mohajeri, R. P. Brooker, M. P. Rodgers, D. K. Slattery, M. D. Hampton, D. A. Cullen, S. Seal, *J. Power Sources* **2013**, *225*, 75.
[29] J. Choi, J. H. Yeon, S. H. Yook, S. Shin, J. Y. Kim, M. Choi, S. Jang, *ACS Appl. Mater. Interfaces* **2021**, *13*, 806.
[30] A. M. Baker, S. M. Stewart, K. P. Ramaiyan, D. Banham, S. Ye, F. Garzon, R. Mukundan, R. L. Borup, *J. Electrochem. Soc.* **2021**, *168*, 024507.
[31] H. Y. Jung, J. W. Kim, *Int. J. Hydrogen Energy* **2012**, *37*, 12580.
[32] R. Narducci, P. Knauth, J. F. Chailan, M. L. di Vona, *RSC Adv.*. **2018**, *8*, 27268.
[33] P. C. Ma, N. A. Siddiqui, G. Marom, J. K. Kim, *Composites, Part A* **2010**, *41*, 1345.
[34] M. Sianipar, S. H. Kim, Khoiruddin, F. Iskandar, I. G. Wenten, *RSC Adv.* **2017**, *7*, 51175.
[35] F. v. Ferreira, L. P. Souza, T. M. M. Martins, J. H. Lopes, B. D. Mattos, M. Mariano, I. F. Pinheiro, T. M. Valverde, S. Livi, J. A. Camilli, A. M. Goes, R. F. Gouveia, L. M. F. Lona, O. J. Rojas, *Nanoscale* **2019**, *11*, 19842.
[36] G. L. Goh, N. Saengchairat, S. Agarwala, W. Y. Yeong, T. Tran, *Nanoscale* **2019**, *11*, 10603.
[37] C. W. Visser, Y. Tagawa, C. Sun, D. Lohse, *Soft Matter* **2012**, *8*, 10732.
[38] G. H. Lim, K. Ahn, S. Bok, J. Nam, B. Lim, *Nanoscale* **2017**, *9*, 8938.
[39] M. Vinothkannan, R. Hariprasad, S. Ramakrishnan, A. R. Kim, D. J. Yoo, *ACS Sustainable Chem. Eng.* **2019**, *7*, 12847.
[40] J. Zhao, Z. Tu, S. H. Chan, *J. Power Sources* **2021**, *488*, 229434.
[41] J. J. Giner-Sanz, E. M. Ortega, V. Pérez-Herranz, *Int. J. Hydrogen Energy* **2014**, *39*, 13206.
[42] C. H. Lee, H. B. Park, Y. M. Lee, R. D. Lee, *Ind. Eng. Chem. Res.* **2005**, *44*, 7617.